SUPPORTING INFORMATION

Photo-spintronics: Magnetic field-controlled photoemission and light-controlled spin transport in hybrid chiral oligopeptide-nanoparticle structures

Prakash Chandra Mondal[†], Partha Roy[†], Dokyun Kim[‡], Eric E. Fullerton[‡], Hagai Cohen[§], and Ron Naaman[†*]

[†]Department of Chemical Physics, Weizmann Institute of Science, Rehovot 76100, Israel

[‡]Center for Memory and Recording Research, University of California, San Diego, California 92093, USA

[§]Chemical Research Support, Weizmann Institute of Science, Rehovot 76100, Israel

Materials

Biphenyl-4,4′-dithiol, 4-aminothiophenol, 1,16-hexadecane dithiol, $K_4Fe(CN)_6$, $K_3Fe(CN)_6$, and KCl were purchased from Sigma-Aldrich and used without further purification. N-terminal oligopeptides (purity >98%) were purchased from Genemed Synthesis, Inc. (TX, USA) and used as received. Single crystal silicon wafers (400 Ω/cm^2) of 525 ± 25 μm thickness (300 nm of thermal oxide on the surface) were purchased from University Wafers, Inc. All metals (Ta, Pt, Co, and Au) were purchased from Kurt J. Lesker. Core-only CdSe nanoparticles having a diameter of 6.2-7.7 nm (purity >99%) were obtained from MK Nano (ON, Canada) and stored at 4^oC before use.

Magnetic characterization of the substrates

The less coercive value obtained from the multilayer substrates indicates its soft magnetic behavior (Fig. S1).

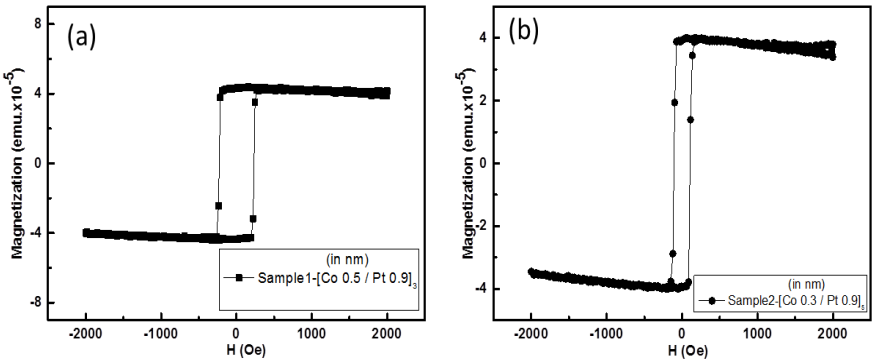

Figure S1. Hysterisis of perpendicular-magnetized ferromagnetic multilayers (a) $Si/SiO_2/Ta_5/Pt_2/(Co_{0.5}\text{-}Pt_{0.9})_5/Co_{0.5}/Au_1$ (sample 1) and (b) $Si/SiO_2/Ta_5/Pt_2/(Co_{0.3}\text{-}Pt_{0.9})_5/Co_{0.3}/Au_1$ (sample 2). Thickness (in nm) of each component is mentioned in the subscript. Magnetic field strength, H (in Oe) is shown along the x-axis, whereas the degree of its magnetization (in emu/cm^3) is shown along the y-axis.

Polarization modulation-infrared reflection-absorption spectroscopy (PM-IRRAS)

The formations of the helical oligopeptide monolayers of Ala8 and Ala8-CdSe nanoparticle structures on the soft ferromagnetic substrates were confirmed by PMIRRAS spectra. For example, the vibrational stretching frequency of the amide-I and amide-II bond was estimated to be at 1672 cm^{-1}, 1542 cm^{-1} (Ala8), and at 1677 cm^{-1}, 1544 cm^{-1} (Ala8-CdSe NPs), respectively, which unequivocally indicates the intactness of the helical structures both in

Ala8 monolayers and Ala8-CdSe NP assemblies (Fig. S2). These result well matches with existing reports.[S1-S3] Moreover, the tilt angle (θ), the helical axis with respect to the substrate normal can be calculated from the amide-I to amide-II peak intensity ratio.[S4] Interestingly, the SAMs of Ala-8 showed a tilt angle, θ, of ~54±2°, whereas that of Ala8-CdSe was observed at ~36±0.5°. A decrease in θ by 18° revealed that not only the NPs become attached; it also facilitates the monolayer in keeping it upright with respect to the surface normal. A significant enhancement was found in the intensity of the N-H vibration observed at 3328 cm^{-1} after CdSe adsorption, as compared with its monolayer (Fig. S2b). Full-width at half-maxima (FWHM) was found to decrease by ~66 cm^{-1} in the Ala-NP hybrid structure compared with that of monolayers, which might be the result of breaking the intermolecular hydrogen bonding after CdSe-NH_2 formation. Both the Ala8 and Ala8-CdSe nanoparticle architectures display strong peaks at 2924 and 2854 cm^{-1} that are related to the asymmetric and symmetric stretching vibrations of methylene (-CH_2-), respectively (Fig. S2b). The vibrational studies confirm the formation of monolayers and their nanoarchitectures.

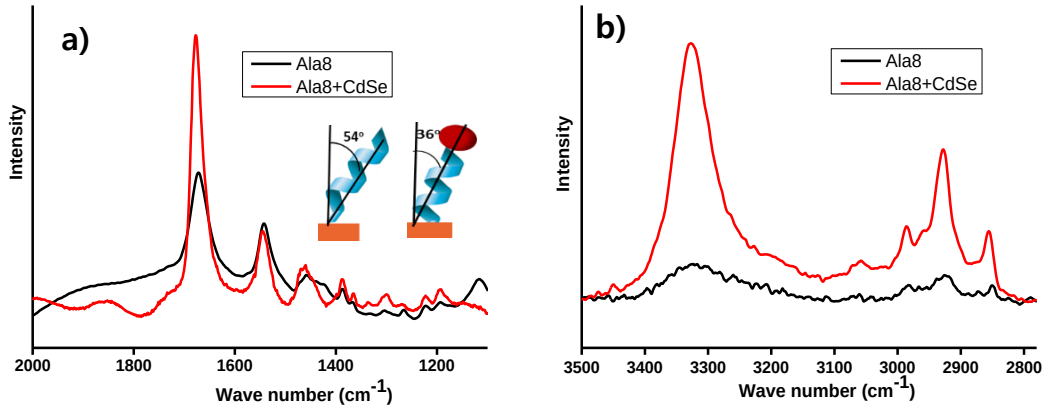

Figure S2. PM-IRRAS spectra of Ala8 (black line) and Ala8-CdSe NP structures (red line) were recorded in two different regions, a) the amide-I (1672, 1675 cm^{-1}) and amide-II (1542, 1544 cm^{-1}) region, and b) the N-H (~3250-3400 cm^{-1}), and C-H (~2800-3000 cm^{-1}) vibrational regions, respectively.

Atomic force microscopy (AFM) imaging of Ala8-CdSe

The AFM image of CdSe NPs assembled over the polypeptide monolayers on the ferromagnetic substrates exhibited a homogenous distribution and the surface coverage was found to be 40±5% (Fig. S3).

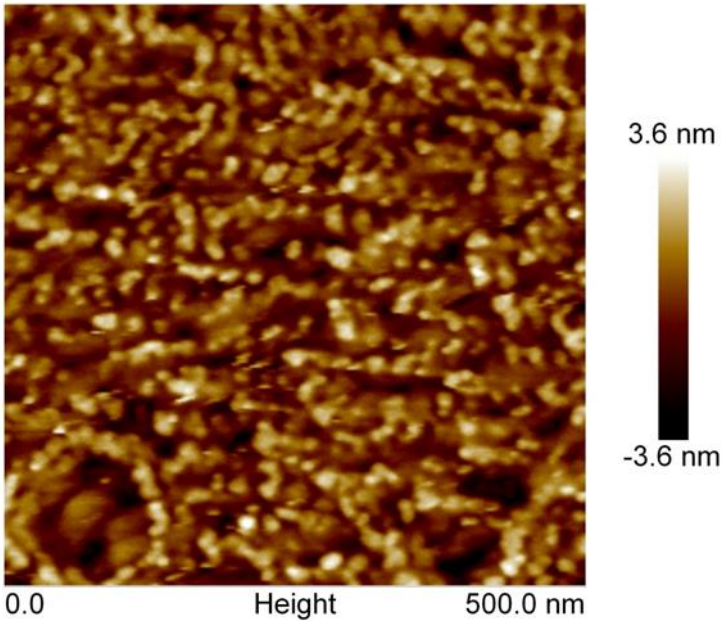

Figure S3. AFM topographical images of Ala8-CdSe nanoparticle assemblies prepared over ferromagnetic substrates. The scan area was 500 nm × 500 nm.

X-ray photoelectron spectroscopy (XPS) measurements

Elemental analysis of the ferromagnetic multilayered substrate

X-ray photoelectron spectroscopy (XPS) data analysis was performed with the help of literature values.[S5] Substrate signals of oxygen and the four constituting metals were quantified. Specifically, the Ta 4f line consists of two doublets with the Ta $4f_{7/2}$ peaks at 22.25 and 23.46 eV, assigned to metallic and oxidized Ta (TaO_x) states, respectively (Fig. S4a). From the intensity dependence on the emission angle (not shown), we infer that Ta-oxide is formed on top of the metallic Ta. The binding energy of this oxidized state is far from the range of literature values (e.g., around 26.6 eV for TaO_x), a fact that may point to charge transfer effects between the ultra-thin layers. Indeed, all metal binding energies (see Table S1 and Fig. S4) differ from the corresponding literature values of bulk metals. The Pt $4f_{7/2}$ and metallic-Ta $4f_{7/2}$ peaks appear both at energies higher than the corresponding literature values, whereas the Au $4f_{7/2}$ and metallic-Co $2p_{3/2}$ peaks are both at binding energies lower than the literature values. The Co signal is dominated by oxide species, but a metallic component is clearly observed (indicated by an arrow in Fig. S4c), in agreement with the presence of magnetic signals, as demonstrated in Figure S1. The relatively small signal of metallic Co is due to the inherent surface sensitivity of the XPS probe, and it does not contradict the possibility of having significant amounts of metallic Co. Note that the bare substrate exhibits

a much higher metallic Co intensity than that of the modified Co. Complementarily, an oxygen signal originating from the metal oxides is resolved in the O 1s spectrum; hence, it can be quantified, as presented in Table S2 (see below).

A very thin overlayer of metallic Au (nominally ~1 nm) is derived from the Au 4f doublet appearing at 83.9 and 87.6 eV, ascribed as $4f_{7/2}$ and $4f_{5/2}$, respectively (Fig. S4d). Assuming a uniform coverage, the thickness of this gold overlayer is estimated to be only ≤0.5 nm, which may indicate the emergence of partial diffusion into the inner layers, or alternatively, slight clustering and non-uniformity within the gold layer itself.

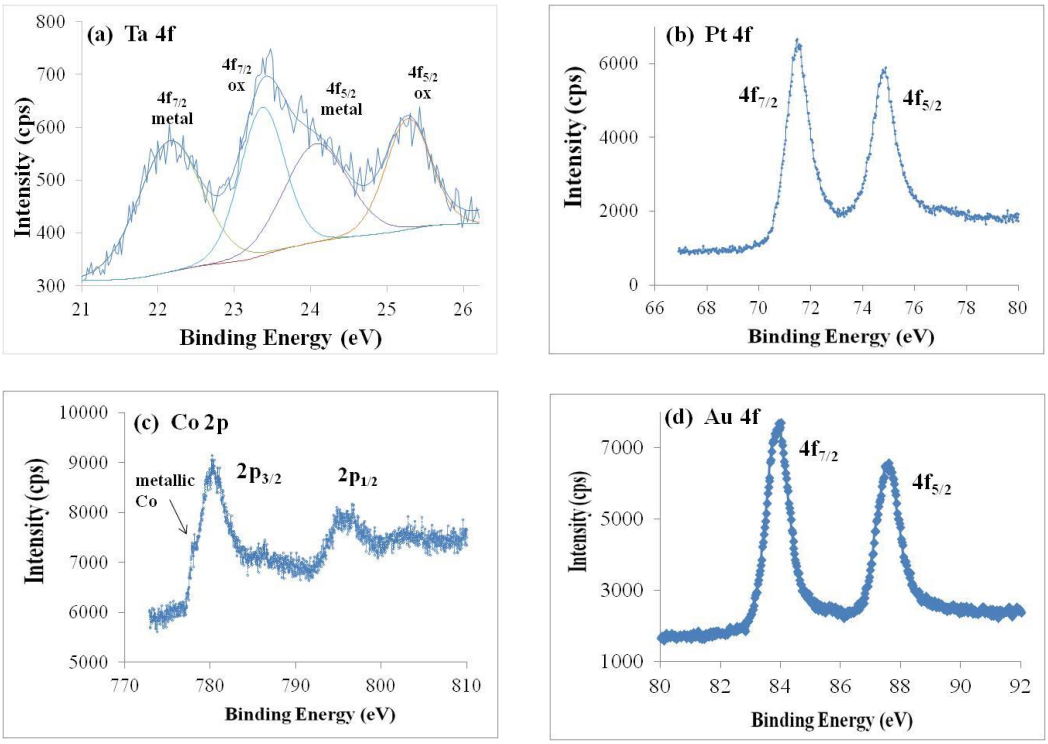

Figure S4. XP spectra of the Ta 4f (a), Pt 4f (b), Co 2p (c), and Au 4f (d) in the pristine ferromagnetic multilayer substrates. Characteristic emission peaks are denoted. The metallic Co $2p_{3/2}$ peak is specifically indicated by an arrow in Fig. 4c.

XPS analysis of the oligopeptide monolayers

The chemical composition derived for oligopeptide monolayers over the ferromagnetic substrate is summarized in Table S2. Two well-resolved components of oxidized carbon (indicated by an arrow in Fig. S5c) are shown, attributed to oxidized-C states within the molecules. Their binding energies and intensities are in agreement with the theoretical expectation (see Tables S2 and S3). Based on the chemical compositions in the sample, good agreement with the expected values of the total C/N and N/S elemental ratios was found; however, with extra C that is situated on top of the monolayer and also with a small amount of oxidized sulphur, S(Ox) contamination, presumably SO_4. The analysis of the oligopeptide monolayer in samples with NPs is more involved, due to overlapping signals of organic species that arise from the NPs. However, the results are generally in agreement with those of samples without NPs, as detailed in Table S2.

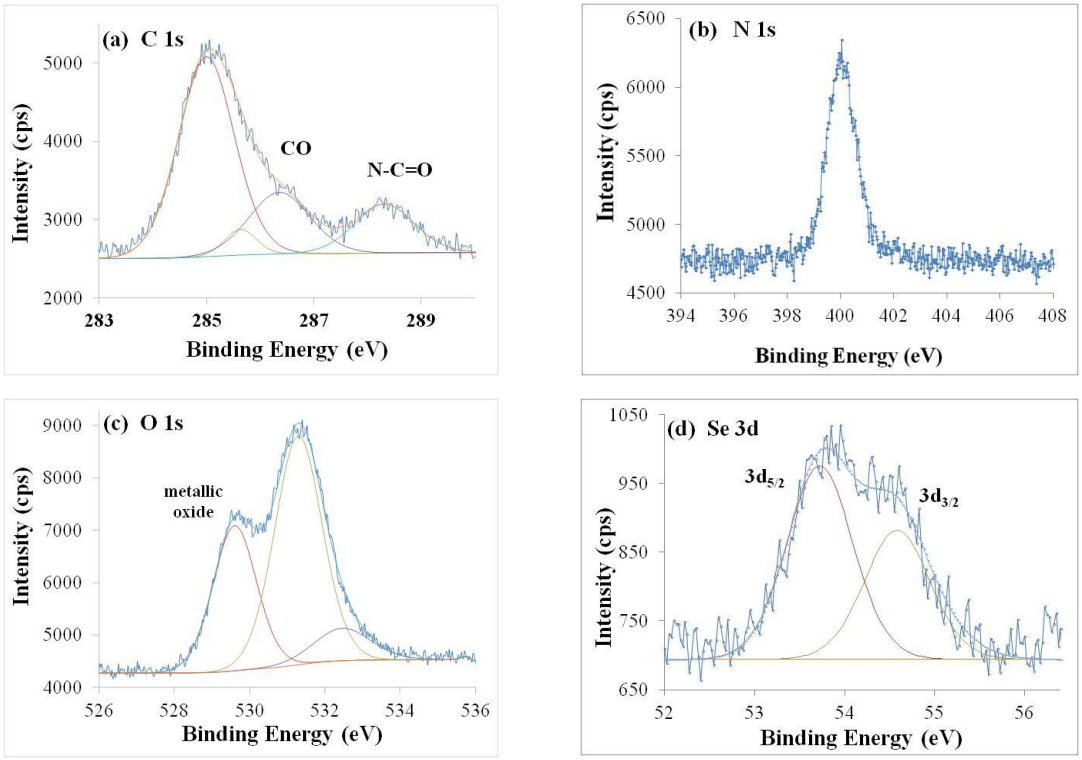

Figure S5. XP spectra of the C 1s (a), N 1s (b), O 1s (c) and Se 3d (d) in the Ala8 and Ala8-CdSe NP overlayers. Selected peaks are denoted.

Table S1. Binding energies (in eV) of the main XPS lines. Rows 2 and 3 correspond to oxidized states. Deviations from the common literature values are attributed to mutual charge transfer effects among the ultra-thin layers. Some reference literature values are given in brackets.

B.E	Au	Pt	Ta	Co	O	C	N	S	Cd	Se
1	83.89 (84.0)	71.47 (71.2)	22.25 (21.9)	777.87 (778.3)	529.61	284.90	400.00	163.5	405.12	54.12
2			23.46	779.85	531.3	286.42		168.15		
3					532.5	288.20				

XPS analysis of the oligopeptide–CdSe NP structures

The NPs consist of a CdSe core (6-7 nm in diameter and an ideal stoichiometry of 1:1), plus a shell of oxidized Cd that is believed to be mainly $Cd(OH)_2$. This shell gives rise to an elemental ratio of Cd/Se > 1. Based on the data in Table S2, the thickness of this passivated-Cd shell is estimated to be 1-1.4 nm, depending on the actual shell composition (e.g., CdO or $Cd(OH)_2$). On top of this shell, a second shell is formed by a capping agent, octadecyl amine (H_2N-$(CH_2)_{17}$-CH_3, which is ~2.4 nm in thickness. Taking the latter into account, we estimate the coverage by NPs to be around 25-30% of the surface, which is in reasonable agreement with our independently derived AFM values, as discussed earlier. In fact, the estimated coverage is believed to be even larger than 30%, because the organic contaminants detected here (see Table S2) seem to reside preferentially on the NPs, which would alter the calculation towards higher coverage values.

In practice, *the active core* of these NPs applies to only a small part of the calculated coverage. This core is probably ≤5 nm in diameter, which accounts volume-wise to only about 10-15% of the NPs' surface coating.

Chemically resolved electrical measurements (CREM)

Our CREM data provide two useful inputs. First, Table S3 depicts work function (WF) values recorded at a very early stage of the experiment, representing the fresh, irradiation-free samples. Both values are lower than the WF value of gold and, moreover, a slight decrease in WF was found under the deposition of NPs. The latter change is believed to be locally even more pronounced, because the WF values represent a large averaging area. Hence, we expect the spontaneous emergence of a vertical field, in order to promote electron transport from substrate to NPs across the helical oligopeptide.

A direct observation of this tendency is given by our CREM inspection of the response to light illumination, using a LED source with λ=630 nm. Figure S6 shows how the Cd line shifts under illumination to lower binding energies as compared with the value recorded in the dark. This effect is reversible (shifting back upon switching the light off) and it was measured with three different substrates prepared under identical conditions. Notably, it was not observed for the molecular layer domains in between the NPs. Therefore, it reflects the *local* photovoltage right on the NP surface, owing to the preferred transport of excited holes (as compared with excited electrons) from NPs to substrate via the helical oligopeptide monolayers. This latter result provides a useful reference to our photoluminescence and electrochemical data, as discussed in the main text.

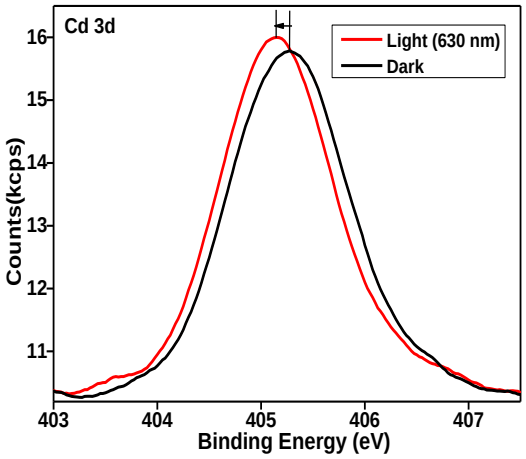

Figure S6. Light induced XPS for oligopeptide-NP hybrid structures. The red curve corresponds to the Cd $3d_{5/2}$ XPS line measured under illumination by light with λ=630 nm. The black curve shows the spectrum under dark conditions. An arrow indicates the light-induced difference in binding energies, yielding here ~120 meV.

Table S2. Composition summary: The elemental atomic percentage (%), decomposed into the various sample domains. M corresponds to the integral signal of substrate metals. Values in brackets correspond to theoretical expectations.

		N	C	O	M	Cd	Se	C^{OO}:C^{O}:N
Without NPs	**Substrate**			9.70	21.07			
	Mol. Layer	9.12	32.05	16.62				0.95 : 1.15 : 1 (1 : 1 : 1)
	contamination		7.8	2.75				
With NPs	**Substrate**			5.13	22.19			
	Mol. Layer	5.1	16.72	9.35				1.35 : 1.74 : 1
	NPs			2.50		2.59	1.34	
	NP capping	0.59	13.0					
	contamination		14.3	7.21				

Table S3. Main XPS and CREM results, including representative atomic concentration ratios, estimated layer thicknesses, work function (WF), and the photovoltage (PV) values extracted from the Cd line.

Composition	**C/N**	**N/S^{red}**	**O^{org}/N**	**Cd/Se**	**d^{org} (A)**	**d^{Au} (A)**	**WF (eV)**	**PV-Cd (meV)**	**PV-Au (meV)**
Without NPs	4.1 (±20%)	19 (±20%)	2.1 (±10%)	---	39 (±10%)	5 (±30%)	4.48	---	---
Theoretical	3.3	18	1.83	---	30	10			
With NPs	7.7	--	1.82	1.93		5	4.375	120	<3

Photoluminescence measurements (PL)

CdSe NPs bound to achiral monolayers of either a 4,4'-biphenyl dithiol monolayer or 4-aminothiophenol did not show any spin-dependent photoluminescence behavior, as the change is minimal which could be in the limit of experimental error (Fig. S7).

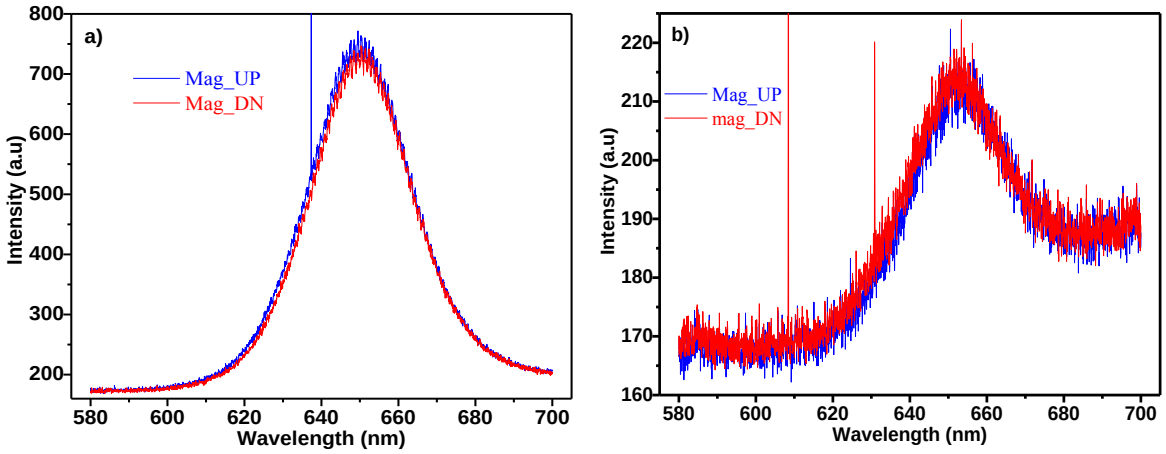

Figure S7. Spin-dependent photoluminescence spectra of CdSe NPs attached to the 4,4'-biphenyl dithol monolayer (a) and the 4-aminothiophenol monolayer (b) over ferromagnetic substrates measured in the presence of an external magnetic field of 0.35 T either magnetic moment pointing "UP" (solid blue curve), or "DOWN" (solid red curve), and measured under identical conditions. Nanoparticles were excited with a green laser at 514 nm.

Controlled spin-dependent electrochemistry without molecules on magnetic substrates

The voltammograms were recorded on a bare ferromagnetic substrate, since a working electrode did not show any magnetic field effect when the working electrode was magnetized either with its magnetic moment pointing "UP" or "DOWN" (Fig. S8).

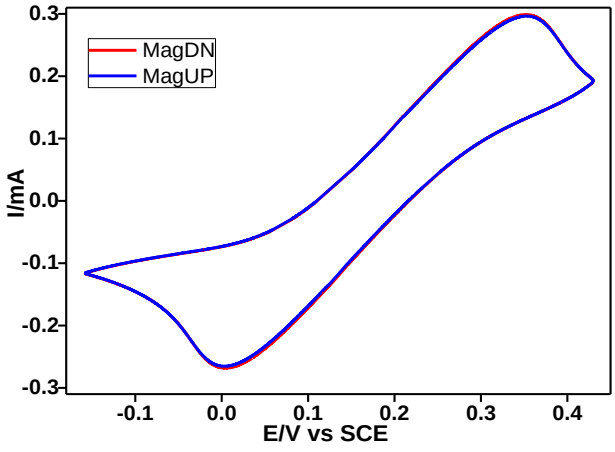

Figure S8. Cyclic voltammograms recorded on bare ferromagnetic electrode. The voltammograms were obtained when the cobalt was magnetized either with its magnetic moment pointing "UP" (solid blue curve) or "DOWN" (solid red curve). The voltammograms were measured in Tris buffer containing 5 mM $K_4[Fe(CN)_6]/K_3[Fe(CN)_6]$ at 50 mV s^{-1}.

REFERENCES

S1. Boncheva, M.; Vogel, H. Formation of stable polypeptide monolayers at interfaces: Controlling molecular conformation and orientation. *Biophys. J*. **1997**, *73*, 1056-1072.

S2. Mandal, H. S.; Kraatz, H. B. Effect of the surface curvature on the secondary structure of peptides adsorbed on nanoparticles. *J. Am. Chem. Soc*. **2007**, *129*, 6356-6357.

S3. Peer, N.; Dujovne, I.; Yochelis, S; Paltiel, Y. Nanoscale charge separation using chiral molecules. *ACS Photonics* 2015, *2*, 1476−1481.

S4. Miura, Y.; Kimura, S.; Imanishi, Y.; Umemura, J. Formation of oriented helical peptide layers on a gold surface due to the self-assembling properties of peptides. *Langmuir* 1998, *14*, 6935-6940.

S5. Moulder, J. F.; Stickle, W. F.; Sobol, P. E; Bomben, K. D. Handbook of X-ray photoelectron spectroscopy, Perkin-Elmer Corp., Eden Prairie, MN, 1992.